



Synthesis and characterization of iron phosphate NPs and applications in magnetically guided drug delivery

Anuradha and Indrajit Roy*

Department of Chemistry, University of Delhi, Delhi-110007, India.

Submitted on: 05-01-2016 Accepted and Published on 07-Feb-2016

ABSTRACT

Microemulsion mediated synthesis has long been used to synthesize nanoparticles of controlled dimensions, with encapsulated active agents. Iron phosphate nanoparticles offer various attractive attributes for medical use. We have synthesized the iron phosphate nanoparticles (FP) using water-in-oil (reverse micelles) microemulsion system. Aqueous core of reverse micelles was used to encapsulate hydrophilic (FITC-Dextran) dye. In vitro analysis showed that these nanoparticles are non-toxic and uptaken by cells; which can be further enhanced upon magnetic guidance. These results highlight the potential for FP to be used as safe and efficient agent for optical bioimaging and magnetically guided drug delivery.

Keywords: Iron phosphate (FP), FITC Dextran (FD), chitosan (CH), magnetic targeting, cytotoxicity.

INTRODUCTION

There are different types of nanomaterials (polymeric, inorganic etc.) which we can use for various applications, such as targeted drug delivery, gene therapy, ultrasensitive biosensing, etc. A promising way of nanoparticle-mediated targeted drug delivery involves guiding the drug-nanoparticle conjugates to target sites using external stimulus, such as light and magnetic field.^{1,2}

Magnetic field assisted drug delivery is highly promising as it involves the use of non-ionizing radiation, with no restriction on their penetration depth across biological tissues. Iron phosphate is one such material having the combination of potentially interesting magnetic properties and drug-carrying capacity. Several new materials in the iron (III) families have recently been synthesized.³⁻⁶ Their ultra-small size, paramagnetic properties, ease of synthesis, and biocompatibility makes them ideally suited for a variety of medical applications.

The most popular application of iron-containing nanoparticles is in contrast enhancement in magnetic resonance imaging

(MRI).⁷⁻¹³ Moreover, their ability to respond to external magnetic field has led to several promising applications, such as magnetic field-directed cell separation and magnetically-targeted drug delivery.^{14,15} Magnetic field assisted delivery of active molecules by iron-phosphate nanoparticles can lead to several medical benefits, which include targeted delivery of chemotherapeutic agents for combination of MRI diagnostics and chemotherapy (theranostics), combination with optical agents for combined MRI and optical imaging, etc.¹⁶

In this work, fluorophore-encapsulated iron-phosphate nanoparticles were synthesized in the microemulsion media. The resulting nanoparticles were characterized for their size, surface functionality and crystallinity, along with their magnetic and optical behaviour. Following that, they were treated with cultured cells to probe their non-toxicity and biocompatibility. Concurrently, their uptake in cells in culture was studied by optical bioimaging. Fluorimetric analysis of lysate of cells treated with fluorophore-doped nanoparticles was used to quantitatively estimate the cellular uptake of nanoparticles. Finally, the effect of external magnetic guidance on the extent of cellular uptake of nanoparticles was probed.

EXPERIMENTAL

Materials

Ferrous chloride, disodium hydrogen phosphate, sodium hydroxide, chitosan (CH), and hexane (AR grade) were purchased from SRL (India). Surfactant Aerosol OT (or AOT), i.e. bis (2-ethylhexyl) sulphosuccinate (AR grade), Fluorescein Isothiocyanato-Dextran (FD), tris-HCl buffer and Triton X-100

Dr. Indrajit Roy

Department of Chemistry, University of Delhi, Delhi-110007, India.

Tel: +11-9560721851

Email: indrajitroy11@gmail.com

Cite as: *J. Mat. NanoSci.*, 2016, 3(1), 1-7.

©IS Publications ISSN 2394-0867 <http://pubs.iscience.in/jmns>

were purchased from Sigma-Aldrich (USA). L-ascorbic acid, ferrozine (3-(2-pyridyl)-5,6-bis(phenyl sulfonic acid)-1,2,4-triazine), neocuproine (2,9-dimethyl(1,10-phenanthroline), ammonium acetate and HCL were purchased from Alfa Aesar. Cell culture media (DMEM), fetal bovine serum (FBS), antibiotics (penicillin and streptomycin), amphotericin B, and MTT Reagent [3-(4, 5-dimethylthiazol-2-yl)-2, 5-diphenyltetrazolium bromide] were obtained from Genetix (India). Lung carcinoma cells lines (A-549) was purchased from ATCC (USA), and cultured according to instructions supplied by the vendor. Unless otherwise mentioned, all other cell culture products were obtained from Thermo Fisher Scientific. All chemicals were used without any further purification. The experiments were carried out at ambient temperature and pressure. The water used for reactions was double distilled.

Methods

Synthesis of FITC-Dextran loaded iron phosphate nanoparticles

FITC-Dextran loaded nanoparticles of iron phosphate were synthesised by carrying out minor modification in the previously reported procedure.¹⁷ Specifically, 0.1 M AOT solution was prepared in hexane. In 25 ml of AOT in hexane, 140 μ l aqueous solution of 1M FeCl₂ and 7.5 μ l aqueous solution of FITC-Dextran (10mg/ml) were added by continuous stirring for 12 hours to form microemulsion A. In another 25 ml of AOT solution, 50 μ l of 0.2M Tris-HCl buffer (pH 7.4), 70 μ l aqueous solution of 0.1M Na₂HPO₄ and 7.5 μ l aqueous solution of FITC-Dextran (10mg/ml) were dissolved by continuous stirring for 12 hours to form microemulsion B. Before stirring both the microemulsions, excess water was added to make total volume of water to 450 μ l to adjust w_o , i.e. the molar ratio of water to AOT (should be equal to or less than 10). Both the microemulsions were optically clear solutions. Microemulsion B was then added to microemulsion A at an extremely slow rate (~20 drops per min) with continuous stirring at room temperature. The resulting solution was further stirred for another 12 hours. The entire process of nanoparticles formation is depicted in Figure 1.

Development of translucency indicated the nanoparticle formation in the aqueous core of the microemulsion droplets. Hexane was completely removed from the resulting solution, and the nanoparticles containing the solid mass of AOT was dissolved in 10ml of absolute ethanol (99.9%) by vortexing. The solutions were centrifuged for half an hour at 8000 rpm at room temperature in centrifuge (spin win). The pelleted nanoparticles were washed with absolute ethanol three times. Finally, the pelleted nanoparticles were dispersed in double distilled water at room temperature by vortexing to give stable dispersion.

Synthesis of FITC-Dextran loaded iron phosphate nanoparticles coated with chitosan

FITC-Dextran loaded and chitosan coated nanoparticles of iron phosphate were synthesized by carrying out minor modification in the previously reported procedure. Specifically, 0.1 M AOT solution was prepared in hexane. In 10 ml of AOT in hexane, 84 μ l aqueous solution of 0.1M FeCl₂ and 4.5 μ l aqueous solution of FITC-Dextran (10mg/ml) were added by continuous stirring for 12 hours to form microemulsion in vial A. In another vial B, 10 ml of AOT solution, 30 μ l of 0.2M Tris-HCl buffer (pH 7.4), 42

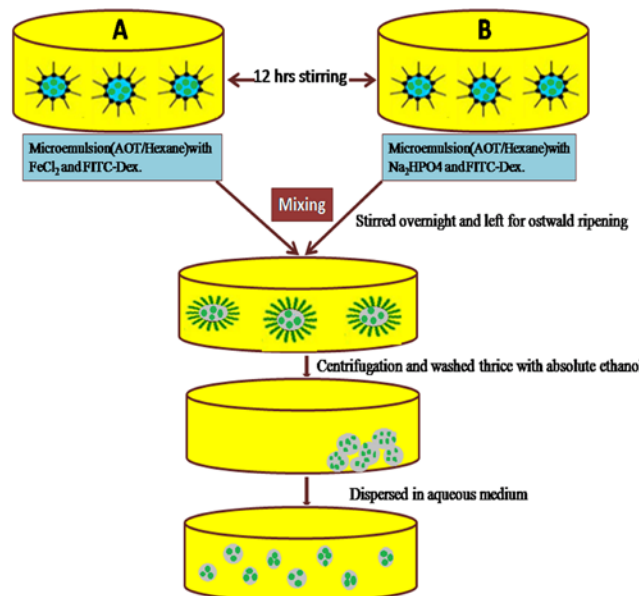


Figure 1. Schematic representation of formation of iron phosphate nanoparticles in the aqueous core of water-in-oil microemulsion.

μ l aqueous solution of 0.1M Na₂HPO₄ and 4.5 μ l aqueous solution of FITC-Dextran (10mg/ml) were added. In vial C, 10 ml of AOT in hexane and 135 μ l aqueous solution of 1% chitosan was added. Vial D also contains 5 ml of AOT in hexane and 135 μ l aqueous solution of 1% Chitosan was added.

Distilled water is added to make the total water to AOT ratio less than 10 i.e. w_o (the molar ratio of water to AOT). All these solutions remained for continuous stirring for 12 hr to form clear microemulsion. All the 4 microemulsions were optically clear solutions. Microemulsion C was then added to microemulsion A at an extremely slow rate (~20 drops per min) with continuous stirring at room temp to make microemulsion A', while microemulsion D was added to microemulsion B at an extremely slow rate (~20 drops per min) with continuous stirring at room temperature to make microemulsion B'. The resulting two microemulsions, i.e. A' and B', were further mixed by drop wise addition as done earlier and remained in stirring for another 12 hr in the room temperature. Development of translucency indicated the nanoparticle formation in the aqueous core of the microemulsion droplets. Then, hexane was completely removed from the resulting solution using rotary vacuum evaporation, and the nanoparticles containing the solid mass of AOT were dissolved in 10 ml of absolute ethanol (99.9%) by vortexing. The solutions were centrifuged for half an hour at 8000 rpm at room temperature in centrifuge (spin win). The pelleted nanoparticles were washed with absolute ethanol three times. Finally, the pelleted nanoparticles were dispersed in double distilled water at room temperature by vortexing to give stable dispersion.

CHARACTERIZATION

The magnetic properties of the dried nanoparticles were probed using vibrating sample magnetometer (VSM), using a Model 3473-60 Electromagnet Amplifier (CREST Performance CPX 900 power amplifier Instrument). The size of the iron phosphate nanoparticles were determined using transmission electron microscopy (TEM). Aqueous dispersion of nanoparticles were

sonicated, drop-coated and dried onto formvar coated 200 mesh copper grids (Ted Pella, USA), followed by imaging using a TECNAI G2-30 U TWIN TEM instrument (FEI, Eindhoven, The Netherlands), with an acceleration voltage of 300 kV. The same instrumentation setup was used for probing the elemental composition (using energy dispersive X-ray spectroscopy, or EDX) of the nanoparticles.

High resolution powder X-ray diffraction (HXRD) was used to analyze the phase composition of the nanoparticles, using a Bruker D8 Discover X-ray spectrometer, over the 2θ range from 10–60, with a step size of 0.020, scan rate of 1.5 second/step, 40 milliamp current and 40KV voltage, using Cu-K α radiation ($\lambda = 1.54060 \text{ \AA}$). The Fourier transform infrared spectroscopy (FTIR) spectra for the prepared nanoparticles were recorded on Perkin Elmer RX1 Instrument. The optical properties (UV-visible absorption and fluorescence emission spectra) of the nanoparticles, with and without encapsulated fluorophore, were recorded using a Shimadzu UV-1601 spectrophotometer (Shimadzu, Kyoto, Japan) and a Cary Eclipse fluorescence spectrometer (Varian, Palo Alto, CA), respectively.

The stability of the fluorophore, both free and nanoencapsulated was studied using a fluorescence quenching experiment. Here, fixed concentrations of free and nanoencapsulated FD in aqueous medium were treated with various concentrations of the chemical quencher Cu²⁺ (copper sulphate).¹⁸ Fluorescence emission intensities in the absence (I_0) and presence (I) of various quencher concentrations was then measured using the Cary Eclipse fluorescence spectrophotometer. A plot was made with the natural log of (I/I_0) versus quencher concentration [Q]. The slope of the plot correlated directly with the extent of chemical quenching of the fluorophore.

The release profile of the fluorophore from the nanoparticles was next probed. Dried FPs loaded with fluorophore FD, with and without chitosan coating, were dispersed in 15 ml of phosphate buffer saline (PBS, pH = 7.4) by simple agitation for 2–3 min. Then, 15ml of the nanoparticles (FD-FP, FD-FP-CH) solution were distributed in 5 vials and was kept at 37°C. At predetermined intervals of time, the solutions were centrifuged and the supernatant was collected. The amount of released FD was determined by measuring the fluorescence intensity of the various supernatant solutions. The corresponding residues (containing nanoparticle-encapsulated FD) were also dispersed in water and analysed for fluorescence.

In vitro studies:

Analysis of potential in vitro cytotoxicity of the nanoparticles:

The human lung cancer cells A-549, were grown in DMEM media, supplemented with 10% fetal bovine serum (FBS), 1% antibiotic penicillin/ streptomycin, and 1% antifungal Amphotericin B. The cells were maintained at 37 °C and 5% CO₂ in a humidified incubator, using standard cell culture procedures and manufacturer's instructions.

For analyzing cell viability upon treatment with nanoparticles, one day prior to treatment, the cells were trypsinized and resuspended in fresh media. 75,000 cells/1 ml fresh media were added to each well of a sterilized 24-well plate, and transferred back to the incubator for attachment and overnight growth. Next day, to the cells at a confluency of about 50%, aqueous dispersion

of the nanoparticles was added, mixed by swirling, and transferred back to the incubator. After two days of incubation, the plate was taken out, and the cells in each well were washed three times with sterile PBS, and treated with 100 μ l of MTT reagent [3-(4,5-dimethylthiazol-2-yl)-2,5-diphenyltetrazolium bromide], (5 mg/ml in PBS)] for 2 hours.¹⁹

The resulting blue-coloured formazan crystals were dissolved in DMSO, and the optical density of this solution was recorded at 570 nm using UV–visible spectrophotometry. The optical density of each solution reflected the viability of the cells in each well. The percentage viability of the treated cells were calculated after comparing their optical density with that of non-treated cells (positive control), the later being arbitrarily assigned 100% viability. The experiment was carried out in triplicates.

Cellular uptake of fluorescence doped nanoparticles in vitro via fluorescence microscopy

Fluorescence microscopy of cells and fluorescence estimation from cell lysates were used to monitor the uptake of the fluorophore-doped nanoparticles in cells. One day prior to treatment, the cells were seeded in sterilized 6-well plates (2,00,000 cells/2 ml fresh media in each well) and returned to the incubator. Next day, to the cells at a confluency of about 70%, aqueous dispersion of fluorophore-doped nanoparticles was added (nanoparticle concentration 2.4 μ M), mixed by swirling, and returned to the incubator. After two hours of incubation, the plate was taken out, the treatment-media aspirated, and cells in each well were washed twice with sterile PBS. The washed cells were fixed by washing with methanol, followed by addition of 50 % glycerol. The fixed cells were then analysed using a fluorescence microscope (ZEISS Axiovert 40 CFL).

The quantitative estimation of uptake of FD-doped FPs in cells via fluorescence analysis of cell lysates was carried out by a similar procedure as above. Here, after nanoparticle treatment and subsequent washing of cells with PBS, as described above, the cells were lysed by adding 200 μ l of cell lysis reagent (1 % Triton X-100 in water) to each well of the 6-well plate, followed by incubation for 30 min with gentle shaking. After this, the cells in the lysis solution were scraped with a sterile scraper, and mixed with an additional 1 ml of PBS in each well. Then, the mixtures were transferred to microcentrifuge tubes (maximum capacity 1.5 ml). The cell debris was separated from the lysate by centrifugation (3,000 rpm, 5 min). The supernatant (centrifugate) was collected for analysis of FD fluorescence in the spectrofluorimeter.

Analysis of cellular uptake of nanoparticles in vitro via estimation of iron content from the cell lysates

For analyzing in vitro nanoparticle uptake in cells upon treatment with iron phosphate nanoparticles, one day prior to treatment, A-549 lung cancer cells were trypsinized and suspended in fresh media. Then, about 1,00,000 cells/mL media were added to sterilized 35 mm single-well plates, and transferred back to the incubator for attachment and overnight growth. Next day, to the cells at a confluency of 80–85%, three different dosages of the iron phosphate, with and without chitosan coating, were added, mixed by swirling, and transferred back to the incubator. For each dosage added, magnetic guidance was provided to three plates by placing a bar magnet below the plates,

while other three plates did not have magnets placed under them (no magnetic guidance). After 10 minutes of treatment, the plates were washed 2-3 times with ice cold phosphate buffer saline (PBS), followed by the addition of 1 mL of hydrochloric acid (10 mM) and incubated (outside the incubator) for 2 hours. The HCl solution not only helped in lysing the cells, but also dissolved the iron phosphate nanoparticles (which are internalized by the cells) to their ionic (Fe^{2+}) form. After scratching the cells, 400 μL of freshly prepared iron determination reagent (IDR) was added to each plate and left for 30 minutes and finally the absorbance was recorded at 560 nm.²⁰

The IDR reagent was prepared by mixing the following solutions in water by shaking for 2-3 minutes: 2.5 M of ammonium acetate, 1 M of L-ascorbic acid, 6.5 mM ferrozine (3-(2-pyridyl)-5,6-bis (phenyl sulfonic acid)-1,2,4-triazine) and 6.5 mM neocuproine (2,9-dimethyl(1,10-phenanthroline)). The ferrozine in the IDR reagent reacts with Fe^{2+} and forms a colored product, with absorbance maxima at 560 nm. The absorbance value obtained from the cell lysate mixtures directly correlates with the Fe^{2+} content from the cell lysates. The absorbance obtained from the cell lysate mixtures were correlated with the Fe^{2+} concentrations, with the help of a previously drawn calibration curve involving absorbance and corresponding Fe^{2+} content.

Analysis of nanoparticles mediated and magnetically guided drug delivery to cells in vitro via estimation of dye related fluorescence from the cell lysates:

For analyzing the efficacy of magnetically guided drug targeting of cells using iron-phosphate nanoparticles encapsulating FITC Dextran (FD-FP), iron-phosphate nanoparticles encapsulating FITC Dextran and coated with chitosan (FD-FP-CH) were added to cells, with and without a bar magnet placed underneath the plates (with and without magnetic guidance). One day prior to treatment, the cells were trypsinized and resuspended in fresh media. Then, 1,00,000 cells/mL of fresh media were added to each well of sterilized 24 well plates, and transferred back to the incubator for attachment and overnight growth. Next day, to the cells at a confluency of 80–85%, three samples were added, mixed by swirling, and transferred back to the incubator. After two hours of treatment, the cells were washed three times with PBS, and fixed volume of cell lysis reagent (prepared by dissolving 1% mass/volume of surfactant Triton X-100 in PBS, pH 7.2) was added to each well and mixed thoroughly. After 30 minutes, the lysates were transferred to microcentrifuge tubes, centrifuged to separate the cell lysates, and the supernatant analysed for fluorescence of FITC-Dex (FD). Higher intensity of FD fluorescence coincides with higher nanoparticle uptake by the cells.

RESULTS AND DISCUSSION

The TEM image, elemental composition, and diffraction pattern of the synthesized iron phosphate nanoparticles are shown in Figure 2 (A, B, and C, respectively). TEM image showed that the diameter of the nanoparticles varied in the range of 20 and 50 nm, with irregular, ‘grain-like’ shape.

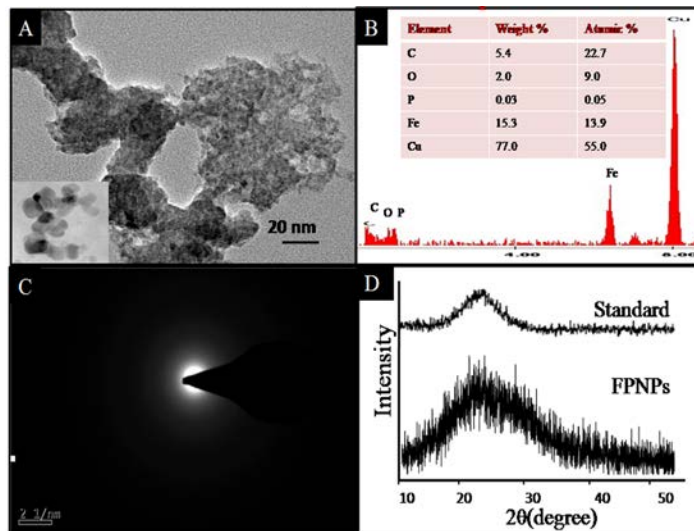


Figure 2. (A) TEM image of FP, (B) EDX spectra of FP, (C) diffraction pattern of FP, and (D) XRD spectrum of iron phosphate nanoparticles (With standard).

Result of EDX analysis of the nanoparticles confirms the elemental composition of these nanoparticles, containing carbon, oxygen, phosphorous and iron. EDX data also show the presence of copper, which is a contamination from the grid. The diffraction pattern shows that these particles are not purely crystalline in nature.

Powder XRD patterns of iron phosphate nanoparticles (FP) is shown in Figure 2 (D). The low crystalline result obtained from the study is compared with the work published by E. Palacios et al.²¹ No other impurity was observed in the XRD pattern. Overall, the poor crystalline nature of the FP can be ascribed due to low temperature synthetic procedure.²²

FTIR spectra of (A) standard FPNPs, (B) synthesized iron phosphate (FP) nanoparticles, (C) iron phosphate coated with chitosan (FP-CH), and (D) chitosan (CH) are shown in Figure 3.

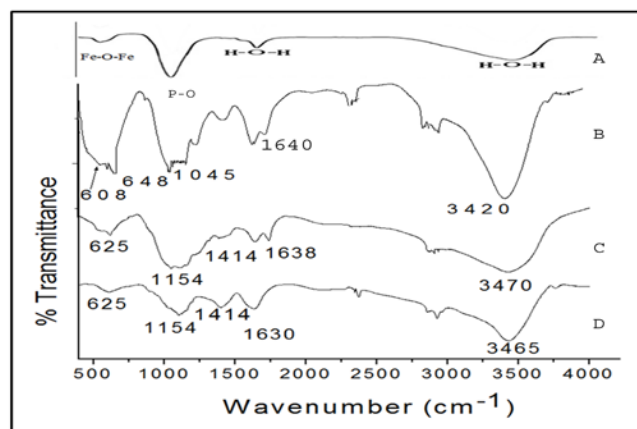


Figure 3. (A) FTIR spectra of standard FPNPs (B) synthesized iron phosphate NPs (FP), (C) iron phosphate NPs coated with chitosan (FP-CH), and (D) chitosan (CH).

In FP (B), peaks at 648 cm^{-1} (Fe–O–Fe) and 1045 cm^{-1} (Fe–O–P) are observed; these are characteristic peaks of iron phosphate.²³ The sharp peaks in the range of $3400\text{--}3500\text{ cm}^{-1}$ were attributed to the stretching vibration of the lattice OH⁻ ion.²⁴⁻²⁶ The doublet in the range $1000\text{--}1150\text{ cm}^{-1}$ was assigned to P–O antisymmetric

stretching mode.²⁷ FTIR spectrum of FP coated with CH (C) shows that the characteristic peaks of iron phosphate and CH move apparently upon chemical interaction with each other. The peaks at 1154 cm^{-1} and 625 cm^{-1} (D) relate to the crystallinity (crystallinity is a function of the degree of deacetylation) of chitosan (CH).²⁸

The disappearance of -OH group of iron phosphate and the movement of polar groups of CH suggest that the hydroxyl ions on the surface of iron phosphate might interact with the plentiful amino and hydroxyl ions of CH via hydrogen bonding.^{29,30} Overall, this study confirms that interaction of CH with the nanoparticles.

The magnetic behaviour of the FP and FP-CH nanoparticles was measured at room temperature using vibrating sample magnetometry (VSM). Under a large external field, the magnetization of the particles aligns with the field direction and reaches its saturation value for both these nanoparticles. The pattern is typical of paramagnetic nanoparticles, as shown in Figure 4.

The saturation magnetization (M_s) values of FP and FP-CH nanoparticles were 0.15 and 0.10 emu/g , respectively. The decrease in saturation magnetization was most likely due to the existence of coated materials and impurities on the surface of the magnetic nanoparticles.³¹

The optical properties of aqueous solutions of FD and FD encapsulated FP (FD-FP) have been studied by UV-visible and fluorescence spectroscopies; their results are provided in Figure 5.

It was observed that FD, both in the free (FD) and nanoencapsulated (FD-FP) forms, have an absorption maxima of 490 nm (Figure 5 A). The fluorescence spectra ($\lambda_{\text{excitation}} = 490\text{ nm}$) at normalized absorption shows that the emission intensity of free FD is reduced upon nanoencapsulation (FD-FP) (Figure 5 B).

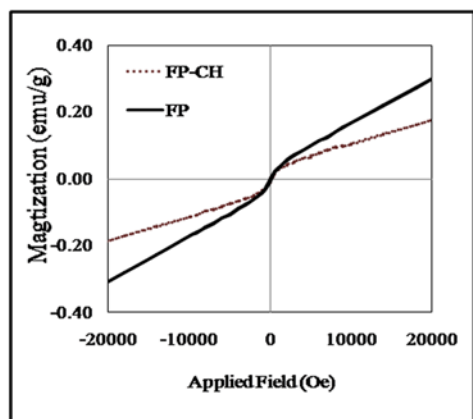


Figure 4. VSM Spectra of FP and FP-CH.

This data shows that the optical properties of the fluorophore are retained in their doped form. We further investigated whether nanoencapsulation enhances the stability of the fluorophore FD against chemically-induced fluorescence quenching. From Figure 5 (C), it is clear that the free fluorophore is more sensitive to chemical quenching than the nanoencapsulated fluorophore, as evident from the steeper fluorescence quenching curve of the former.

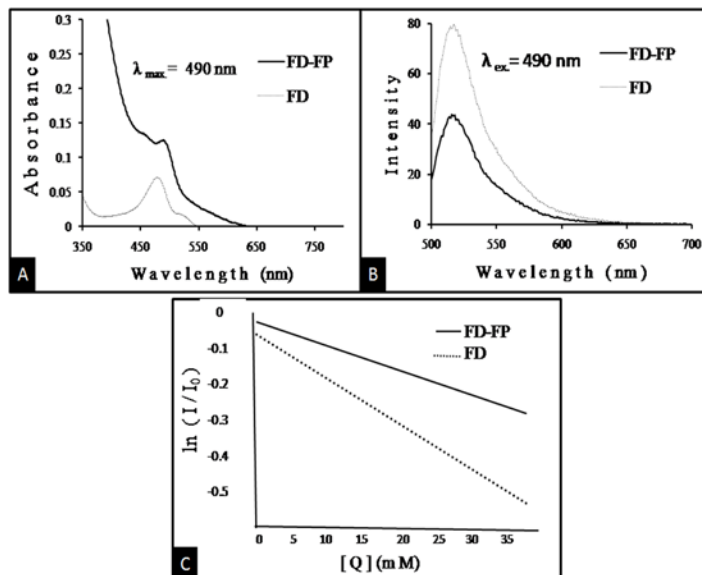


Figure 5. (A) Absorption, and (B) emission spectra of FD and FD-FP. (C) Comparative fluorophore quenching study of FD in free (FD) and nanoencapsulated (FD-FP) form.

However, it is also evident that nanoencapsulation cannot completely prevent the chemical quenching of the fluorophore, but rather provide a relatively enhanced optical stability over the free fluorophore.

Overall, it can be concluded that although the emission intensity of the fluorophore is reduced upon nanoencapsulation, it becomes more stable against chemical quenching in its encapsulated form.

Next, we probed the release profile of the fluorophore from the nanoparticles, the results of which are shown in Figure 6(A). It can be seen that the fluorophore is released from the nanoparticles in a sustained manner, with 50% release in four days. This suggests that these nanoparticles can act as drug delivery vehicles; though their release profile needs further optimization via better tuning of their composition. Similar result was obtained when chitosan coated FP NPs were used; the difference was observed only in release rate. Release was enhanced with chitosan coating (90%) in four days as shown in Figure 6 (B).

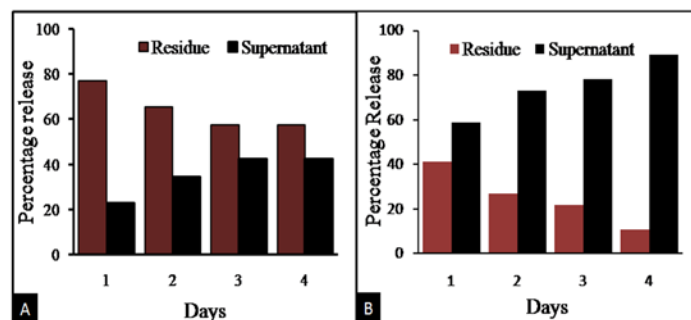


Figure 6. (A) Release pattern of FD from (A) FD-FP nanoparticles, and (B) FD-FP-CH nanoparticles.

Following these characterization studies, we probed the interaction of these nanoparticles with cells *in vitro*, using A-549 cells. First, fluorescence microscopic results demonstrated the qualitative uptake of fluorophore-doped nanoparticles in the cells

(Figure 7). After that, we used spectrofluorimetric analysis of lysates of nanoparticles treated cells to quantitatively probe the cellular uptake of the nanoparticles. Here, cells were treated with FD-doped FP nanoparticles, with two types of surface properties, i.e. without (FD-FP) and with (FD-FP-CH) chitosan coating.

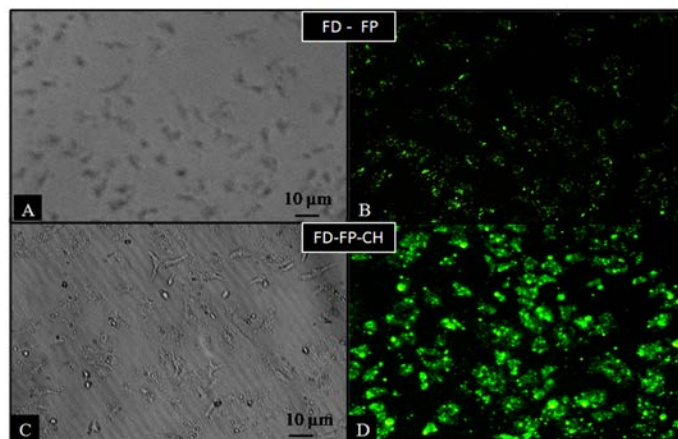


Figure 7. Microscopic images of cells treated with (A, B) FD-FP, and (C, D) FD-FP-CH. (A, C): phase contrast images, and (B, D) fluorescence images.

Figure 8(A) shows that the cellular uptake of the nanoparticles varied with change in surface property, with the chitosan-coated nanoparticles showing higher uptake. These observations can be explained by the fact that the cationic amino groups present in chitosan helps in favourable interaction of the coated nanoparticles with the outer anionic leaflet of cellular membranes. This interaction results in enhanced cellular uptake via endocytosis.³²

After that, in order to study the biocompatibility and non-cytotoxicity of the nanoparticles, we have treated A-549 cells with these nanoparticles (at three different dosages: high, medium and low) for two days, and analyzed the cell viability. It can be seen from Figure 8 (B) that after 48 hours of nanoparticle-treatment, the cells remained about 90-95 % viable in all the dosages tested, with relatively higher viability for the lower dosages. Moreover, chitosan coating of nanoparticles does not discernibly alter the viability of the treated cells. This data demonstrates that the nanoparticles exert negligible toxic effect on the cells, and can be used in biological applications.

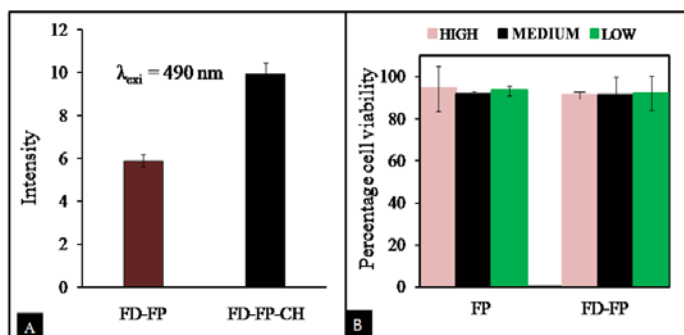


Figure 8. (A) Quantitative estimation of fluorescence recovered from lysates of cells treated with FD-FP and FD-FP-CH (B) Cell viability (MTT) assay of FP and FP-CH (High: 100 μg/ml, Medium: 50 μg/ml, Low: 25 μg/ml).

The above experiments showed that the FD-FP and FD-FP-CH nanoparticles are passively taken up by cells in vitro, with no sign of non-specific toxicity. Next, we probed whether this cellular uptake can be further enhanced via magnetic guidance, as these nanoparticles were found to respond to external magnetic field. Here, we analyzed the nanoparticle uptake within cells using two methods (a) quantitative estimation of total iron content from lysates of cells treated with FP and FP-CH and (b) quantitative estimation of FITC-Dextran related fluorescence from lysates of cells treated with FD-FP and FD-FP-CH.

In each experiment, one set of cells had a bar magnet placed underneath (for magnetic guidance), while the other set of cells did not (no magnetic guidance). The data shows that the use of magnetic field has led to appreciable increase in intracellular iron content, for 10 minutes of treatment with FD-FP-CH. The result of quantitative estimation of intracellular FITC-Dextran fluorescence using spectrofluorimetric assay is presented. The data shows that the use of magnetic field has led to an appreciable increase in intracellular FITC Dextran-fluorescence, for 10 minutes of treatment with FD-FP and FD-FP-CH. These two above results (shown in abstract) confirmed that magnetic guidance can lead to sufficient increase in intracellular uptake of iron-phosphate nanoparticles. Magnetic field experienced by coated NPs is less as compared to plain FPNPs, hence they shows slightly less reaction to external magnetic field because of shielding by the coating.

CONCLUSION

This report describes the synthesis, characterization and in vitro use of FITC-Dextran encapsulated paramagnetic iron-phosphate nanoparticles, with and without chitosan coating. These nanoparticles can encapsulate organic fluorophore and protect them from chemical quenching. These particles have some paramagnetic properties, which is used for magnetically directed drug delivery. Furthermore, it was found that these nanoparticles are well uptaken by cells in culture, which can be further enhanced upon magnetic guidance. These nanoparticles were found to be non-toxic to cells. These experiments suggest that these nanoparticles can serve as a non-toxic magnetically targeted drug delivery vehicle.

ACKNOWLEDGMENTS

We are grateful to University of Delhi, India, for providing R&D Grant to support this study. Financial support from Department of Biotechnology (DBT), India, in the form of a research grant is also appreciated.

REFERENCES

- P.N. Prasad, Introduction to Biophotonics. Wiley: New York, 2004.
- C.S.S.R Kumar, W. Hansel, W. Soboyejo, J. Zhou and J. Hormes. LHRH-conjugated magnetic iron oxide nanoparticles for detection of breast cancer metastases. *Breast Cancer Res. Treat.* **2006**, 99, 163.
- J.R.D. Debord, W. M. Reiff, C. J. Warren, R. C. Haushalter, Zubieta. A 3-D Organically Templated Mixed Valence ($\text{Fe}^{2+}/\text{Fe}^{3+}$) Iron Phosphate with Oxide-Centered $\text{Fe}_4\text{O}(\text{PO}_4)_4$ Cubes: Hydrothermal Synthesis, Crystal Structure, Magnetic Susceptibility, and Mössbauer Spectroscopy of $[\text{H}_3\text{NCH}_2\text{CH}_2\text{NH}_3]_2[\text{Fe}_4\text{O}(\text{PO}_4)_4]$. *J. Chem. Mater.*, **1997**, 9, 1994-1998.
- J.R.D. Debord, W. M. Reiff, R. C. Haushalter, Zubieta. The first organically templated layered iron phosphate-hydrothermalsynthesis, structure,

- magnetic-properties, and the mossbauer spectrum of $[\text{H}_3\text{NCH}_2\text{CH}_2\text{NH}_3](0.5)[\text{Fe}(\text{OH})(\text{PO}_4)]$. *J. Solid State Chem.* **1996**, 125, 186-191.
5. M. Cavellec, D. Riou, G.Ferey.Oxyfluorinated microporous compounds: XI. Synthesis and crystal structure determination of ULM-10, the first bidimensional mixed-valence iron fluorophosphate with intercalated ethylenediamine. *J. Solid State Chem.*, **1994**, 112, 441-447.
 6. K.H. Lii, Y.-F. Huang. Large tunnels in the hydrothermally synthesized open-framework iron phosphate (2)[Fe-4(OH)(3)(HPO₄)(2)(PO₄)(3)]center-dot-xh(2)O *Chem. Commun.*, **1997**, 839-840.
 7. P.J. Caravan, J. Ellison, J. McMurry, RB. Lauffer. Gadolinium(III) Chelates as MRI Contrast Agents: Structure, Dynamics, and Applications. *Chem Rev.*, **1999**, 99, 2293-2352.
 8. S. Aime, L. Frullano, SG. Crich. Compartmentalization of a gadolinium complex in the apoferritin cavity: A route to obtain high relaxivity contrast agents for magnetic resonance imaging. *Angew Chem Int Edn.*, **2002**, 41, 1017-19.
 9. S. Laurent, L.E. Vander, F. Yanjun, R.N. Muller. Synthesis and Physicochemical Characterization of Gd-DTPA-B(sLex)A, a New MRI Contrast Agent Targeted to Inflammation. *Bioconjugate Chem.*, **2004**, 15, 99-103.
 10. S. Geninatti, A. Barge, E. Battistini, C. Cabella, S. Coluccia, D. Longo, V. Mainero, G. Tarone, S. Aime. Magnetic resonance imaging visualization of targeted cells by the internalization of supramolecular adducts formed between avidin and biotinylated Gd³⁺ chelates. *J Biol Inorg Chem.*, **2005**, 10, 78-86.
 11. B.S. Chhikara, S. Kumar, N. Jain, A. Kumar, R. Kumar. Perspectivity of bifunctional chelating agents in chemical, biological and biomedical applications. *Chem. Biol. Lett.*, **2014**, 1(2), 77-103.
 12. T. Kupka, JO. Dziegielewski, G. Pasterna, JG. Malecki.Copper-D-penicillamine complex as potential contrast agent for MRI. *Magn Reson Imaging*, **1992**, 10, 855.
 13. J.A. Davies, S.G. Dutremez, C.M. Hockensmith, R. Keck, N. Richardson, S. Selman, D.A .Smith, C.W. Ulmer, LS. Wheatley. Iron-based second-sphere contrast agents for magnetic resonance imaging: development of a model system and evaluation of iron (III) tris (tironate) complex in rats. *J. Zeiss Acad Radiol*, **1996**, 3,936-945.
 14. L. Levy, Y. Sahoo, K. S. Kim, E. J. Bergey and P. N. Prasad. Nanochemistry: Synthesis and Characterization of Multifunctional Nanoclinics for Biological Applications. *Chem. Mater.*, **2002**, 14, 3715-3721.
 15. M.S. Islam, J. Kurawaki, Y. Kusumoto, M. Abdulla-Al Mamun and M. Z. B. Mukhlsh. Hydrothermal Novel Synthesis of Neck-structured Hyperthermia-suitable Magnetic (Fe₃O₄, γ -Fe₂O₃ and α -Fe₂O₃) Nanoparticles. *J. Sci. Res.*, **2012**, 4, 99-107.
 16. C. Tassa, S. Y. Shaw and R. Weissleder.Dextran-Coated Iron Oxide Nanoparticles: a Versatile Platform for Targeted Molecular Imaging, Molecular Diagnostics and Therapy. *Acc. Chem. Res.*, **2011**, 44, 842-852.
 17. I. Roy, S. Mitra, A. Maitra, S. Mozumdar. Calcium phosphate nanoparticles as novel non-viral vectors for targeted gene delivery. *Int. J. Pharmaceutics.*, **2003**, 250, 25-33.
 18. B. L. Bales and M. Almgren. Fluorescence Quenching Of Pyrene By Copper(II) In Sodium Dodecyl-Sulfate Micelles - Effect Of Micelle Size As Controlled By Surfactant Concentration. *J. Phys. Chem.*, **1995**, 99, 15153-162.
 19. I. Roy, T. Y. Ohulchanskyy, H. E. Pudavar, E. J. Bergey, A. R. Oseroff, J. Morgan, T. J. Dougherty, and P. N. Prasad. Ceramic-based nanoparticles entrapping water-insoluble photosensitizing anticancer drugs: a novel drug-carrier system for photodynamic therapy. *J. Am. Chem. Soc.*, **2003**, 125, 7860-65.
 20. J. Riemer, H. H. Hoepken, H. Czerwinska, S. R. Robinson, and R. Dringen. Colorimetric ferrozine-based assay for the quantitation of iron in cultured cells. *Analytical Biochemistry*, **2004**, 331,370-375.
 21. E. Palacios , P. Leret , J. F. Ferna'ndez , A. H. De Aza ,M. A. Rodn'guez. Synthesis of amorphous acid iron phosphate nanoparticles. *J Nanopart Res.*, **2012**, 14, 1131.
 - 22.W. Zhou, W. He, , X. Zhang , S. Yan , X.Sun , X. Tian, X. Han ,J. Panyam and V. Labhasetwar. Biodegradable nanoparticles for drug and gene delivery to cells and tissue. *Adv. Drug Deliv. Rev.*, **2003**, 55, 329-47
 - 23.N. K. Mal, A .Bhaumik and M. Matsukata.syntheses of mesoporous hybrid iron oxophenylphosphate, iron oxophosphate and sulfonated oxophosphate. *Ind. Eng. Chem. Res.*, **2006**, 45, 7748-7751.
 24. P. Zimmer and J. Kreuter. Microspheres and nanoparticles used in ocular delivery systems. *Adv. Drug Deliv. Rev.*, **1995**, 6, 61-73.
 25. D. H. W. Hubert, M. Jung, P. M. Frederik, P. H. H. Bomans, J. Meuldijk, and A. L. German. Vesicle-Directed Growth of Silica. *Adv. Mater.*, **2000**, 12, 1286-1290.
 26. H. P. Hentze, S. R. Raghavan, C. A. McKelvey, and E. W. Kaler. Silica hollow spheres by templating of cationic vesicles. *Langmuir*, **2003**, 19, 1069.
 27. Z. Gen-Tao, Y. Qi-Zhi, N.Y. Jie, and J. Gu. Formation of aragonite mesocrystals and implication for biomineralization. *Am. Mineral.*, **2009**, 94, 293-302.
 - 28.M. Miya, R. Iwamoto, and S. Mima. FT-IR study of intermolecular interactions in polymer blends *J. Polym. Sci. Polym. Phys.*, **1984**, 22, 1149-1151.
 29. K. Masanori, I. Toshiyuki, I. Soichiro, N. Hiroko, K. Yoshihisa, T. Kazuo, S. Kenichi, and T. Junzo. Biomimetic synthesis of bone-like nanocrystals using the self-organization mechanism of hydroxyapatite and collagen. *Composite Sci. Technol.*, **2004**, 64, 819-825.
 30. C. Xianmiao, L .Yubao , Z. Yi, Z . Li, L. Jidong, and W .Huanan. Properties and in vitro biological evaluation of nano-hydroxyapatite/chitosan membranes for bone guided regeneration. *Mater. Sci. Eng. C.*, **2009**, 29, 29-35.
 31. G. Y, Y. Zhang, J. Xia et al, Effect of surface charge and agglomerate degree of magnetic iron oxide nanoparticles on KB cellular uptake in vitro. *Colloid Surf B Biointerfaces.*, **2009**,73,294-301.
 32. K. Corsi, F. Chellat, L. Yahia, and J. C. Fernandes. Mesenchymal stem cells, MG63 and HEK293 transfection using chitosan-DNA nanoparticles. *Biomaterials*, **2003**, 24, 1255-1264.